

# pH-controlled Release System for Curcumin based on Functionalized Dendritic Mesoporous Silica Nanoparticles

Khaled EA AbouAitah<sup>1</sup>, Farghali AA<sup>2\*</sup>, Anna Swiderska-Sroda<sup>3</sup>, Witold Lojkowski<sup>3\*</sup>, Abdel-Fattah M Razin<sup>1</sup> and Khedr MH<sup>2</sup>

<sup>1</sup>Department of Medicinal and Aromatic Plants Research, Pharmaceutical and Drug Industries Research Division, National Research Centre (NRC), Dokki, Giza, Egypt.

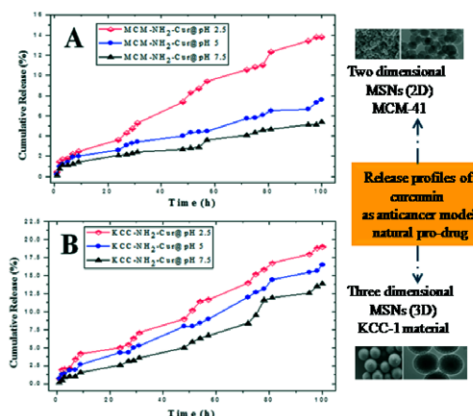
<sup>2</sup>Materials Science and Nanotechnology Department, Faculty of Postgraduate Studies for Advanced Sciences, Beni-Suef University, Beni-Suef, Egypt.

<sup>3</sup>Laboratory of Nanostructures for Photonic and Nanomedicine Institute of High Pressure Physics, Polish Academy of Sciences, Warsaw, Poland

## Abstract

Mesoporous silica materials are promising drug delivery systems, especially in case of poorly water-soluble drugs. Curcumin (Cur) has proven effective for several pharmacological activities including anti-inflammatory, antioxidant, antimicrobial, hepatoprotective, and anticancer activities. In the present work two types of mesoporous silica nanoparticles were evaluated as a Cur carrier for controlled release of this anticancer natural pro-drug: MCM-41 (Two Dimensional) and KCC-1 (Three Dimensional), both functionalized with aminopropyl groups. KCC-NH<sub>2</sub> and MCM-NH<sub>2</sub> contained a similar amount of Cur (24.5% and 23.9%, respectively). *In vitro* experiments have shown that both materials effectively release Cur and the cumulative release was enhanced for low acidity (pH=2.5). At low acidic pH (2.5), the KCC-1 sample released higher amount (up to 19%) of curcumin compared to MCM-41 (14%).

Thus it is possible to achieve controlled, long-term and effective pH-stimulated release of curcumin from amine-functionalized mesoporous silica nanoparticles. This finding opens the way for their application for controlled curcumin delivery in cancer disease because of the acidic tumor environment, increase its stability and lead to an increase of the Cur bioavailability. Moreover, the KCC-1 three dimensional mesoporous silica seems to be a more promising nano-carrier compared to the commonly used MCM-41 material.



**Keywords:** Drug delivery system; pH-controlled release; MCM-41 and KCC-1; Mesoporous silica nanoparticles and curcumin

## Introduction

Drug delivery systems (DDSs) received much attention in biomedical applications. DDSs can improve the bioavailability of poorly water-soluble drugs via preventing premature degradation and enhancing uptake, leading to maintain the desirable controlled drug release and reducing side effects by targeting medicine to specified places [1]. Since mesoporous silica nanoparticles (MSNs) have been reported as a drug delivery systems for the first time [2], they became widely popular inorganic nano-carriers in DDSs [3-12]. MSNs have several attractive properties including their straightforward synthesis, large surface area, porous structure, silanol-containing surface that lead to facile functionalization chemistry, chemical and mechanical stability, biocompatibility and low-toxicity [13-15]. Furthermore, engineering of the surface chemistry and pore dimension can significantly enhance MSNs application in drug delivery systems. Various nanostructured mesoporous silica materials (MSMs) have been developed for controlled release of drugs. Nowadays MCM-41 and SBA-15 are commonly used. New 3D fibrous-structured (KCC-1)

silica was introduced in 2010 [16]. KCC-1 presents an unique fibrous morphology with large surface area and non-ordered pore structure [16], which is of great interest for designing intelligent drug delivery systems and biomedical applications. In present work we examined

**\*Corresponding authors:** Lojkowski W, Laboratory of Nanostructures for Photonic and Nanomedicine, Institute of High Pressure Physics, Polish Academy of Sciences, Warsaw, Poland, Tel: 48228880429; E-mail: [wloj@unipress.waw.pl](mailto:wloj@unipress.waw.pl)

Farghali AA, Materials Science and Nanotechnology Department, Faculty of Postgraduate Studies for Advanced Sciences, Beni-Suef University, Beni-Suef, Egypt, Tel: 48228880429 ; E-mail: [d\\_farghali@yahoo.com](mailto:d_farghali@yahoo.com)

**Received** December 10, 2015; **Accepted** February 01, 2016; **Published** February 10, 2016

**Citation:** AbouAitah KEA, Farghali AA, Swiderska-Sroda A, Lojkowski W, Razin AMF, et al. (2016) pH-controlled Release System for Curcumin based on Functionalized Dendritic Mesoporous Silica Nanoparticles. J Nanomed Nanotechnol 7: 351. doi:10.4172/2157-7439.1000351

**Copyright:** © 2016 AbouAitah KEA, et al. This is an open-access article distributed under the terms of the Creative Commons Attribution License, which permits unrestricted use, distribution, and reproduction in any medium, provided the original author and source are credited.

KCC-1 nanoparticles as a curcumin carrier for the purpose of anticancer therapy. Curcumin is a hydrophobic, polyphenol organic compound, and the principal curcuminoid of turmeric (*Curcuma longa*) medicinal plant [17]. Cur acts as anti-oxidant [18], anti-inflammatory [19], anti-microbial [20] pro-drug. It exhibits anticancer effect in various types of cancers, including: multiple myeloma [21], head and neck squamous cell carcinoma [22], and prostate cancer [23]. Moreover, curcumin is safe at doses even up to 12 g per day [24]. Therefore, Cur was used in various cancer treatments, including colorectal, pancreatic, breast, prostate, multiple myeloma, lung, head and neck, and cancer lesions [25,26]. However, poor solubility, and then poor bioavailability prevents therapeutic efficiencies of curcumin. Finally, in spite of anti-cancer effect, Cur has not been approved as a therapeutic drug for biomedical applications [27]. To achieve maximum therapeutic efficiency of anticancer poorly water-soluble compounds a novel approaches are needed [28]. Among proposed strategies, the nanotechnology is examined to solve the inherent problems such as solubility, stability, toxicity, delivery and bioavailability [29]. Various organic nano-carriers for enhancing the solubility and delivery of Cur, including PLGA nanoparticles, nanosuspensions, cyclodextrin complexation, polymeric nanoparticles liposomes were tested. However, there are several limitations to use such organic-based carriers in DDSs, such their poor stability [30] and its release mechanism based on hydrolysis-induced erosion [31]. It was reported that under acidic pH condition, the stability of Cur increased, because of its conjugated diene structure. Under neutral-basic pH conditions, Cur structure is destructed, which is attributed to the remove of the proton from the phenolic group [32]. On the other hand the amorphous form of Cur displays an enhanced solubility and bioavailability comparing to the crystalline structure [33]. Due to excess thermodynamic characteristics of the amorphous form, a high apparent solubility and dissolution rate can be achieved even in poorly water soluble drugs [34]. As curcumin is a promising pro-drug, a few studies have been reported recently on curcumin delivery based on MSNs. Their aim was to enhance the cytotoxicity of curcumin and exploit the effect of surface functionality on cellular uptake and anticancer activity when utilizing the MCM-41 type [35,36], as well as curcumin-loaded guanidine for combating breast cancer using KIT-6 silica type [37] and controlled release of curcumin from hollow silica material [38,39]. However, to the best of our knowledge no reports on utilization of KCC-1 silica type in delivery of curcumin as model anticancer natural pro-drugs yet reported, and also no comparative study to analyze the differences between the KCC-1 material and commonly used MCM-41 type in controlled release of the small molecule drugs has been carried out. In the present paper we intend to test if, contrary to previous reports on delivery of curcumin, the utilization of KCC-1 dendritic mesoporous silica nanoparticles could be of great significance as nanocarrier.

In the light of the above considerations, we report a comparative study of a simple and efficient pH-controlled release of Cur using the 3D dendritic fibrous mesoporous silica (KCC-1) compared with well-known 2D silica material (MCM-41).

## Materials and Methods

### Materials

Cetyltrimethylammonium bromide (CTAB, Fluka), Tetraethyl orthosilicate (TEOS, 98%, Aldrich), sodium hydroxide (Sigma-Aldrich), cetylpyridinium bromide (CPB, Aldrich), cyclohexane (Sigma-Aldrich), iso-propanol (Sigma-Aldrich), acetone (Alpha Chemica, India), ethanol (Sham lab), methanol (Alpha Chemica), 3-Aminopropyltriethoxysilane (APTES 99%, Sigma-Aldrich), toluene

anhydrous (POCH, Poland), dimethylsulfoxide/HPLC grade (DMSO, Tedia, USA), Urea (Sigma-Aldrich), phosphate buffer saline (PBS), curcumin (Sigma-Aldrich) and ultrapure water (18.2 M $\Omega$ , Millipore) were used for the preparation of all aqueous solutions.

### Synthesis of MCM-41 nanoparticles

Two dimensional hexagonal mesoporous silica nanoparticles were synthesized according to previously reported method [40] with a slight modification. In a typical synthesis, CTAB (500 mg) was dissolved in ultrapure water (240 ml) with 2 M of sodium hydroxide solution (1.750 ml) under vigorous stirring for 1 h. Then the mixture solution was heated up 85°C, and after ensuring that the temperature of the solution was stabilized, 2.5 ml of TEOS was slowly added dropwise into the solution over 5 min., and TEOS was allowed to hydrolyse for 2 h. After completion of the synthesis reaction, the solution was cooled down to room temperature. The particles were collected by centrifugation and washed several times with absolute methanol, and dried at room temperature for 12 h. To remove the template surfactant molecules from the mesopores, the as-synthesized material was calcined at 600°C for six hours in air. The resulting material was labelled as MCM-Calcined.

### Synthesis of KCC-1 material

The three dimensional mesoporous silica nanospheres with fibrous and dendritic pore networks were prepared for the first time by Polshettiwar et al. [16] by means of the hydrothermal method. After that, Moon et al. [41] modified the procedure to synthesize mesoporous silica without the hydrothermal process to produce KCC-1 silica nanospheres. We prepared the silica material following this method with some modifications. In a typical synthesis, 1 g of cetylpyridinium bromide and 0.6 g of urea were dissolved in 30 ml of ultrapure Millipore 18.2 M $\Omega$  under stirring during 30 min. Subsequently, 30 ml of cyclohexane and 1.2 ml of isopropanol were added to the solution. With vigorous stirring, 2.7 ml of TEOS was slowly added dropwise to the mixed solution over 5 min. After 30 min of vigorous stirring at room temperature, the reaction mixture was heated up to 85°C, and this condition was maintained for 17 h. In order to collect the silica particles, the reaction mixture was centrifuged and washed with acetone and water several times. Nanoparticles were then dried at room temperature during 12 hours. To remove the surfactant template as-synthesized materials were calcined at 600°C for six hours in air. The resulting material was labelled as KCC-Calcined.

### Post-synthesis functionalization of mesoporous silica materials with amines groups

The amine-functionalized silica materials were prepared using a slightly modified method presented in [42] by reacting the KCC-Calcined and MCM-Calcined with anhydrous toluene. To graft aminopropyl groups on the mesopore's exterior and interior surface of the KCC-1 and MCM-41 calcined-silica materials, the samples were first dried at 50°C for 12 h to remove the physically adsorbed water. Subsequently 1 g of the KCC-Calcined or MCM-Calcined were dispersed in anhydrous toluene (100 ml). In the next step 1.5 ml of APTES was added and the mixture was stirred at room temperature for 24 h. The solid products were obtained by centrifugation. Nanoparticles were washed with ethanol three times and then dried for 12 h at room temperature. Finally, samples were heated at 50°C during 12 h in air. The 3-aminopropyl-grafted materials were donated as MCM-NH<sub>2</sub> and KCC-NH<sub>2</sub>.

### Drug loading

In this study, the loading process of Cur was carried out according

to the procedure based on solvent evaporation method [43], with some modifications. This drug loading process involves two steps: one is the initial loading/adsorption, and the second one is evaporation. The binary solvent system (ethanol/DMSO/acetone 1:1:5, respectively) was prepared.

MCM-NH<sub>2</sub> and KCC-NH<sub>2</sub> (300 mg) were added to solvent containing 100 mg of Cur., to obtain mass ratios of drug to silica equal to 1:3. Suspensions were stirred for 12 h at room temperature (first step). After that, the samples were evaporated using the Rotavap (Büchi, Switzerland) with the water bath set at 50°C (second step). Finally, nanoparticles were re-dispersed in water in order to remove unloaded curcumin molecules. The Cur-loaded silica nanoparticles were collected by centrifugation, and then washed several times with water. Finally, the samples were dried in an oven at 40°C. The resulting materials were denoted as MCM-NH<sub>2</sub>-Cur and KCC-NH<sub>2</sub>-Cur.

### *In vitro* release

*In vitro* release tests were done in phosphate saline buffer (PBS) during 100 h. Typically, 25 mg of MCM-NH<sub>2</sub>-Cur or KCC-NH<sub>2</sub>-Cur were dispersed in 35 ml of PBS buffer solution adjusted to different pH values (2.5, 5 and 7.5). The solutions were stirred at 37°C for 100 h. At predetermined intervals of times, 1.5 ml aliquots were taken to detect present Cur concentration (cumulative release). The aliquots were centrifuged to eliminate silica nanoparticles from solution. Liquid samples (after centrifugation) were analyzed using UV-Vis spectroscopy at  $\lambda=428$  nm. The experiments were conducted in duplicate, and obtained results were averaged. Usually, in order to maintain a constant volume of the solvent during release tests, each time after sampling for analysis (e.g. UV-Vis), adequate volume of fresh medium (without drug-loaded material) is added. In such procedure a calculation procedure is needed to determine the release profiles. To avoid using such a procedure, we conducted release tests in two containers at the same time and after each sampling current solution was added instead of fresh medium. Subsequently, the amount of Cur released from nanoparticles was calculated according to the simple equation:

Cumulative release (%) is defined as the amount of Cur released into solution/amount of calculated Cur into MSNsX100.

### Characterization techniques

The HR-TEM images were taken using High Resolution Transmission Electron Microscope JEOL, JEM 2100, Japan. The morphology and chemical compositions of the samples were also performed using the Field Emission Scanning Electron Microscope (Zeiss Ultra Plus, Germany) equipped with QUANTAX EDS system, Bruker. Different preparation techniques of the samples were used. The specimens were sputtered with carbon or gold-palladium via a sputter coater (Bal-Tech SCD 005), and chromium via a (Quorum, Q150T ES) prior to imaging. X-ray diffraction (XRD) patterns were recorded on a (PANalytical, X'Pert PRO System) using CuK $\alpha$  radiation in the  $2\theta$  range of 10-100°. Nitrogen adsorption-desorption isotherms were measured at 196°C by using a Quantachrome NOVA Automated Gas Sorption System. Before measurements, the samples loaded with drugs were degassed at 50°C for 24 h, with exception of the samples without drugs, which were degassed at 120°C for 12 h. The specific surface areas were measured based on the BET (Brunauer-Emmett-Teller) method. The pore size distributions were obtained from the adsorption/desorption branches of the isotherms based on the density functional theory (DFT). The total pore volumes were calculated

from the adsorption data at the maximum relative pressure (P/P<sub>0</sub>). TGA analysis was performed on a TGA-50 (Shimadzu, Japan) with a heating rate 10°C/min in air flow to evaluate the loading percent and efficiency. To determine the functional groups and chemical bonding the powder samples were characterized using Fourier transformed infrared (FTIR) spectroscopy (Bruker, Tensor 27) equipped with a Attenuated Total Reflectance (ATR, model Platinum ATR-Einheit A 255). For each ATR-FTIR spectra 100 scans were collected, in the range of 350-4000 cm<sup>-1</sup>. Simultaneous Thermal Analysis (STA) collecting in the same time thermogravimetry (TG) and Differential Scanning Calorimetry (DSC) data were performed using STA 499 F1, Jupiter, Netzsch. Samples weighting ca. 10-20 mg were loaded into alumina pan of the STA unit. Before measurements, the helium flow through the STA furnace chamber was applied during 30 min. The experimental parameters were programmed to reach 700°C with a heating rate of 10°C/min under a helium purge of 60 ml/min. Gasses evolved during thermal experiments were analysed *in situ* thanks to coupling of the STA instrument with FTIR spectrometer. Zeta potential measurements for water suspension of nanoparticles (concentration of 1 mg/ml) were performed at 24°C using a Malvern ZetaSizer (NanoZS). The measurements were performed for samples prepared by variation of pH from 2 to 12.

## Results and Discussions

### Structural and morphological characterization

The structural and morphological features of the prepared samples are shown in Figure 1. SEM observations of the KCC-Calcined material (Figure 1A) shows that the sample consisted of non-aggregated, monodisperse spherical particles, ranging from 200 nm to 500 nm in diameter, formed by dendrimeric fibers. This observation is similar to SEM images from [16,41]. TEM images of KCC-Calcined established well-dispersed nanoparticles with narrow size distribution. In particular, the particles possess an interesting fibrous dendritic structure with fibers coming out from the centre and distributed uniformly in all directions (Figure 1B), which also is consistent with the previous studies related to this material [16,41]. In case of MCM-Calcined, the sample consisted of roughly spherical nanoparticles

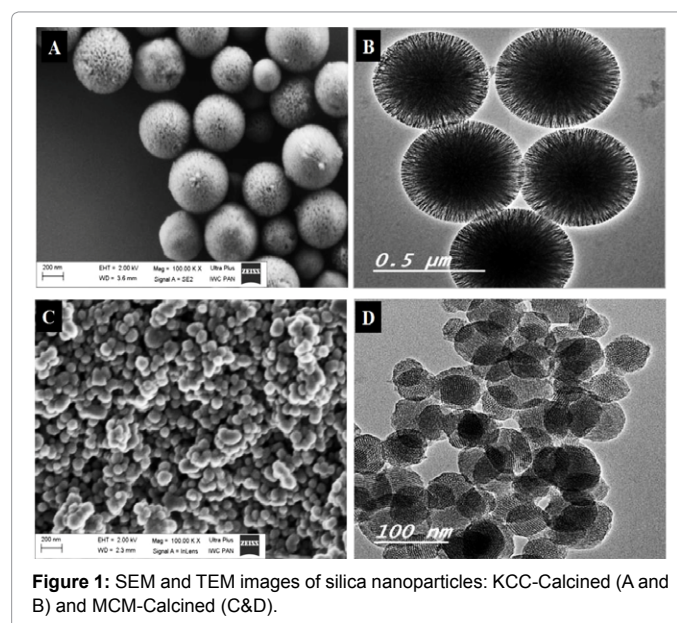


Figure 1: SEM and TEM images of silica nanoparticles: KCC-Calcined (A and B) and MCM-Calcined (C&D).

ranging from 100 nm to 170 nm in diameter, with some aggregation tendency and exhibited hexagonally ordered cylindrical pores (Figures 1C and 1D).

To determine the chemical composition of both silica materials, the Energy-Dispersive X-ray spectroscopy (EDS) analysis was utilized. The materials of MCM-Calcined and KCC-Calcined were composed of silicon and oxygen, which confirmed formation of the silica during the synthesis process (Supporting Information, Figures S1 A and B). On the other hand, amine-functionalized samples of MCM-NH<sub>2</sub> and KCC-NH<sub>2</sub> were composed of silicon, oxygen and nitrogen, which confirmed the successful functionalization of the nanoparticles. However, KCC-NH<sub>2</sub> showed a higher nitrogen content (3.42 wt. %) compared to MCM-NH<sub>2</sub> (2.91 wt. %), as presented in Figures S2 A and B (Supporting information).

### Drug loading and characterization

**N<sub>2</sub> adsorption/desorption analysis:** The successful loading of Cur into pores of the prepared silica nanoparticles was confirmed by nitrogen adsorption/desorption measurements. The N<sub>2</sub> adsorption/desorption isotherms and corresponding pore size distributions in the calcined, functionalized and Cur-loaded samples are shown in Figures 2A and 2B. It can be seen that both types of calcined-nanoparticles had isotherms type-IV, according to the IUPAC classification, confirming their mesoporous structures. The MCM-Calcined presented a single sharp peak, which indicates that this material has a uniform ordered-mesopore structure (Figure 2A). While, the KCC-1 presented a wide peak, which indicate that this material has non-uniform mesoporous structure (Figure 2B). It may be due to the unique pore system with 3D dendritic mesoporous structure [16]. In this context, the MCM-Calcined showed a larger BET surface area than KCC-Calcined sample, 963 m<sup>2</sup>/g and 585 m<sup>2</sup>/g, respectively. Whereas, MCM-calcined material exhibited smaller average pore size diameter than the KCC-Calcined, 2.43 and 3.36 nm, respectively. The data on the calculated textural characteristics of the both nanoparticles before and after drug loading are presented in Table 1. Significant decrease of the surface area, pore volume and pore size of the functionalized and Cur-loaded samples compared to the calcined materials confirms, that the drug molecules indeed filled pore spaces (Figure 2 and Table 1). These results agreed with the previous studies [44-47].

**Determination of drug loading efficiency by TGA analysis:** TGA is an important technique to quantify the drug loading content together with drug loading efficiency in mesoporous silica nanocarriers [45,48]. The aminopropyl functional groups contents were quantified using TGA analysis after correction the TG curve by water content (Figure 3). The amount of aminopropyl groups in MCM-NH<sub>2</sub> and KCC-NH<sub>2</sub> were

5.49 wt.% and 8.92 wt.%, respectively (Table 1). After correcting the TG curve by water and aminopropyl groups contents, the Cur content in MCM-NH<sub>2</sub>-Cur and KCC-NH<sub>2</sub>-Cur were 23.78 wt.% and 24.49 wt.%, respectively (Table 1). Also, the Cur loading efficiency in MCM-NH<sub>2</sub>-Cur and KCC-NH<sub>2</sub>-Cur were 71.41% and 73.57% as presented in Table 1. The results showed that the loading content was slightly higher in KCC-NH<sub>2</sub>-Cur sample compared to MCM-NH<sub>2</sub>-Cur. This is probably due to the larger pore size in the KCC-1 material. Our results confirm earlier statement, that the textural properties such pore size, surface area, pore volume influence significantly drug loading efficiency [15].

**Solid state characterization of materials by XRD and DSC:** The crystalline features of the samples: curcumin, nanoparticles before and after loading of the Cur were characterized by XRD analysis using a fixed angle ranging from 10° to 60° (Figure 4). The crystal diffraction peaks of Cur were clearly observed, the main peak at 17.28°, as well as other intense peaks. For physical mixtures of MCM-NH<sub>2</sub> and KCC-NH<sub>2</sub> with Cur the same crystal diffraction peak of Cur at 17.28° was presented. However, diffraction patterns of MCM-NH<sub>2</sub>-Cur and KCC-NH<sub>2</sub>-Cur did not present any crystalline Cur diffraction peaks. It can be concluded, that Cur had been completely converted to a non-crystalline state. This is consistent with the previous studies [36,46,48]. It was shown that non-crystalline form of the drug placed in mesoporous silica can present increased solubility [45]. Therefore we expect enhanced solubility of Cur in our samples.

The crystalline characteristics of the materials were further achieved by DSC which is considered as a sensitive tool to detect the crystals properties. Information if a crystalline state is still present or

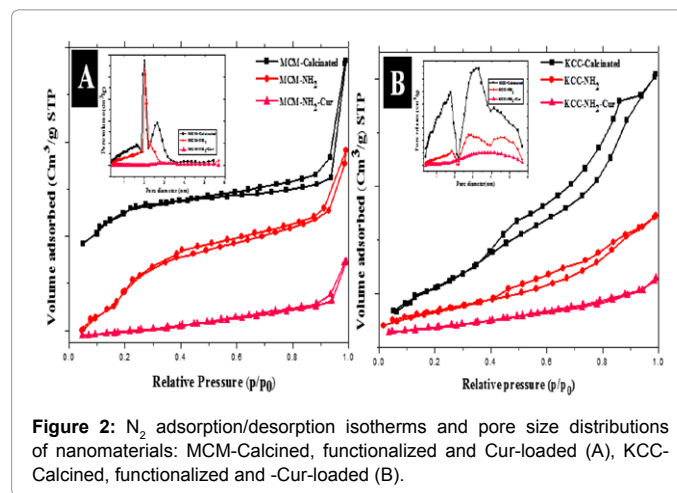


Figure 2: N<sub>2</sub> adsorption/desorption isotherms and pore size distributions of nanomaterials: MCM-Calcined, functionalized and Cur-loaded (A), KCC-Calcined, functionalized and -Cur-loaded (B).

Sample	Surface area (m <sup>2</sup> /g) <sup>BET</sup>	Pore Volume <sup>a</sup> (cm <sup>3</sup> /g)	Pore Size <sup>b</sup> (nm)	Amount of aminopropyl group <sup>c</sup> (wt%)	Nitrogen Content (wt%) <sup>d</sup>	Curcumin loading Content (wt%) <sup>e</sup>	Curcumin Loading efficiency (wt%) <sup>f</sup>
MCM-Calcined	963	0.868	2.43	-	-	-	-
KCC-Calcined	585	0.91	3.36	-	-	-	-
MCM-NH <sub>2</sub>	500	0.75	1.87	5.49	2.91	-	-
KCC-NH <sub>2</sub>	172	0.385	2.88	8.92	3.42	-	-
MCM-NH <sub>2</sub> -Cur	80	0.172	1.642	-	2.24	23.87	71.41
KCC-NH <sub>2</sub> -Cur	88	0.203	2.22	-	2.75	24.49	73.57

<sup>a</sup>Pore volume calculated using DFT theory method.

<sup>b</sup> Pore size calculated using DFT theory method.

<sup>c</sup> Calculated from TGA analysis.

<sup>d</sup> Obtained from EDS analysis

<sup>e</sup> & <sup>f</sup> Calculated from TGA analysis.

Table 1: Physicochemical properties of calcined and functionalized silica materials and drug-loaded of samples.

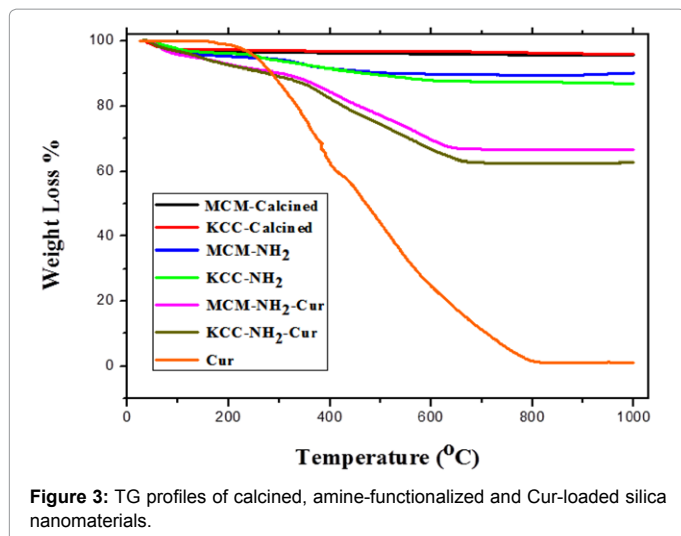


**Figure 3:** TG profiles of calcined, amine-functionalized and Cur-loaded silica nanomaterials.

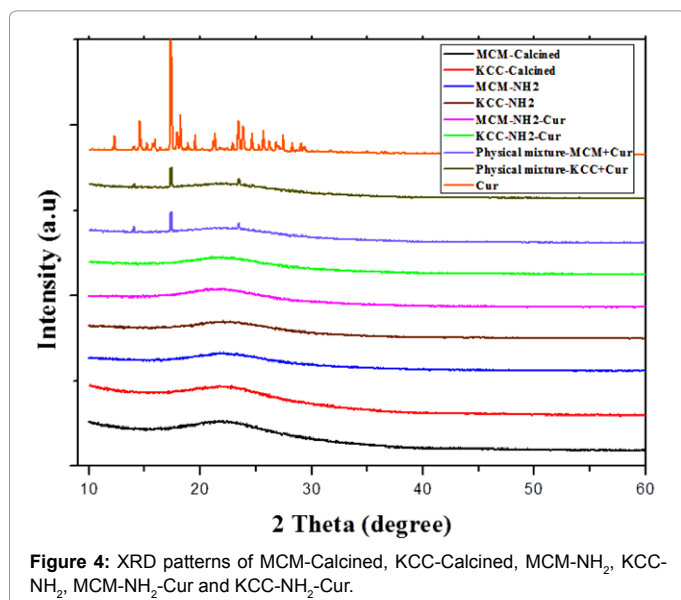


**Figure 4:** XRD patterns of MCM-Calcined, KCC-Calcined, MCM-NH<sub>2</sub>, KCC-NH<sub>2</sub>, MCM-NH<sub>2</sub>-Cur and KCC-NH<sub>2</sub>-Cur.

not, can be obtained from depression of the melting point as a standard means [46]. As shown in Figure 5, the pure curcumin presented a single endothermic melting peak at 183°C. However, the MCM-Calcined, KCC-Calcined, MCM-NH<sub>2</sub>, KCC-NH<sub>2</sub>, MCM-NH<sub>2</sub>-Cur and KCC-NH<sub>2</sub>-Cur did not show endothermic melting peaks at 183°C. It means that the Cur had been completely converted to a non-crystalline state when it was loaded into amine-functionalized silica materials. These results were in consistent with the results of a previous studies obtained by [45,46,48,49]. The DSC results confirmed the XRD characterization. Hence, from the XRD and DSC results, we could conclude that the Cur was loaded into mesoporous silica nanoparticles in non-crystalline state.

**FTIR spectroscopy:** FTIR analysis is employed to investigate the interaction between the drug molecules of Cur and the amine-functionalized MSNs of different morphologies. The FTIR spectra of MCM-Calcined, KCC-Calcined, MCM-NH<sub>2</sub>, KCC-NH<sub>2</sub>, MCM-NH<sub>2</sub>-Cur, KCC-NH<sub>2</sub>-Cur., and pure Cur are shown in Figure 6. In order to show the changes of surface chemistry of different state of samples only

selected range of FTIR spectra are shown. MCM-Calcined and KCC-Calcined showed the wide absorption bands in the range of 3750 to 3000 cm<sup>-1</sup> due to the O-H stretching vibration of water (Figure 6A) [45,47]. Presence of water was due to defective Si-OH on the surface, so that water molecules could be adsorbed and retained by hydrogen bonding. Both calcined materials exhibited one peak at 3747 cm<sup>-1</sup> assigned to silanol groups (ν(O-H)) [50]. As presented in Figure 6, there are several important peaks related to formation of silica nanoparticles, the large peaks in the 1000-1250 cm<sup>-1</sup> range were attributed to Si-O-Si vibrations [51]. Peaks assigned to Si-OH at 810 cm<sup>-1</sup>, Si-O at ~450 cm<sup>-1</sup> are also seen [52]. These signals are not observed for pure curcumin (Figure 6). Removal of surfactants was confirmed by the disappearance of the typical alkyl C-H stretching frequencies at 2850 cm<sup>-1</sup> and 2922 cm<sup>-1</sup> in MCM-Calcined and KCC-Calcined [53].

FTIR spectra of functionalized-mesoporous silica exhibit quite similar features of silica framework with additional several peaks, characteristic for amino groups (Figures 6B and 6C). In the MCM-NH<sub>2</sub> and KCC-NH<sub>2</sub> samples, a band at 686 cm<sup>-1</sup> due to the bending of N-H was detected. The C-N stretching vibration is normally observed in range of 1000-1200 cm<sup>-1</sup>, however, due to the overlay with the IR absorptions of Si-O-Si in the range 1130-1000 cm<sup>-1</sup> and of Si-CH<sub>2</sub>-R in the range 1250-1200 cm<sup>-1</sup>, this peak was not observed in this region [54]. A peak at 1556 cm<sup>-1</sup> was attributed to the symmetrical protonated form of amino groups (-NH<sub>3</sub><sup>+</sup>) bending, which confirmed the existence of amino groups [44,50]. Nevertheless, the peak in this region for the amine-modified samples with APTES is broader, indicating possible overlap of peaks. In addition, the peak at 1650 cm<sup>-1</sup>, which can be assigned to N-H bending, is intensive for the MCM-NH<sub>2</sub> and KCC-NH<sub>2</sub> which would indicate the presence of N-H groups. Strong vibrational peaks were also seen in the C-H stretching region around 2900 cm<sup>-1</sup> in MCM-NH<sub>2</sub> and KCC-NH<sub>2</sub> (Figure 6C) [51,55]. Furthermore, the results obtained by FTIR for amine-modified materials proved the efficiency of the functionalization of the mesoporous silica.

Cur spectrum (Figure 6) indicated that it existed in the keto-enol tautomeric form because bands in the most significant carbonyl region from 1800 to 1650 cm<sup>-1</sup> were detected [56]. Cur exhibited several peaks, one at 806 cm<sup>-1</sup> due to γ(CH) of aromatic and skeletal CCH [57], a band of peaks was observed in region (1000-1300 cm<sup>-1</sup>) which can be

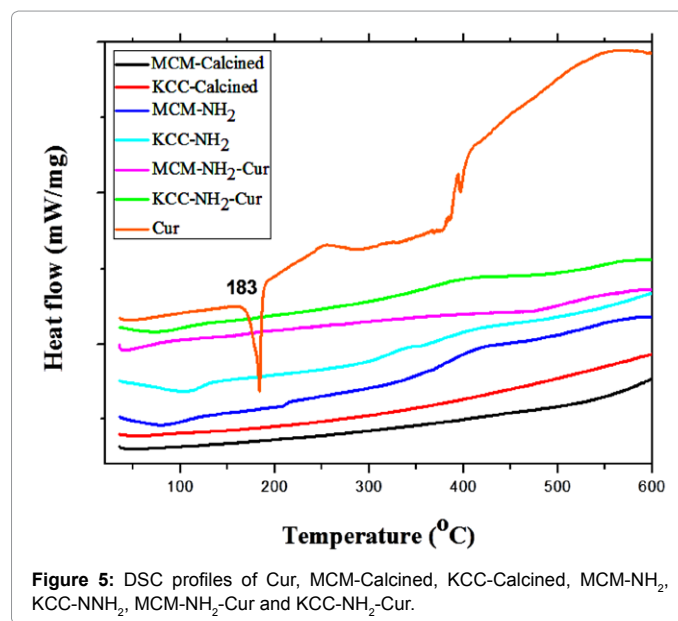


**Figure 5:** DSC profiles of Cur, MCM-Calcined, KCC-Calcined, MCM-NH<sub>2</sub>, KCC-NH<sub>2</sub>, MCM-NH<sub>2</sub>-Cur and KCC-NH<sub>2</sub>-Cur.

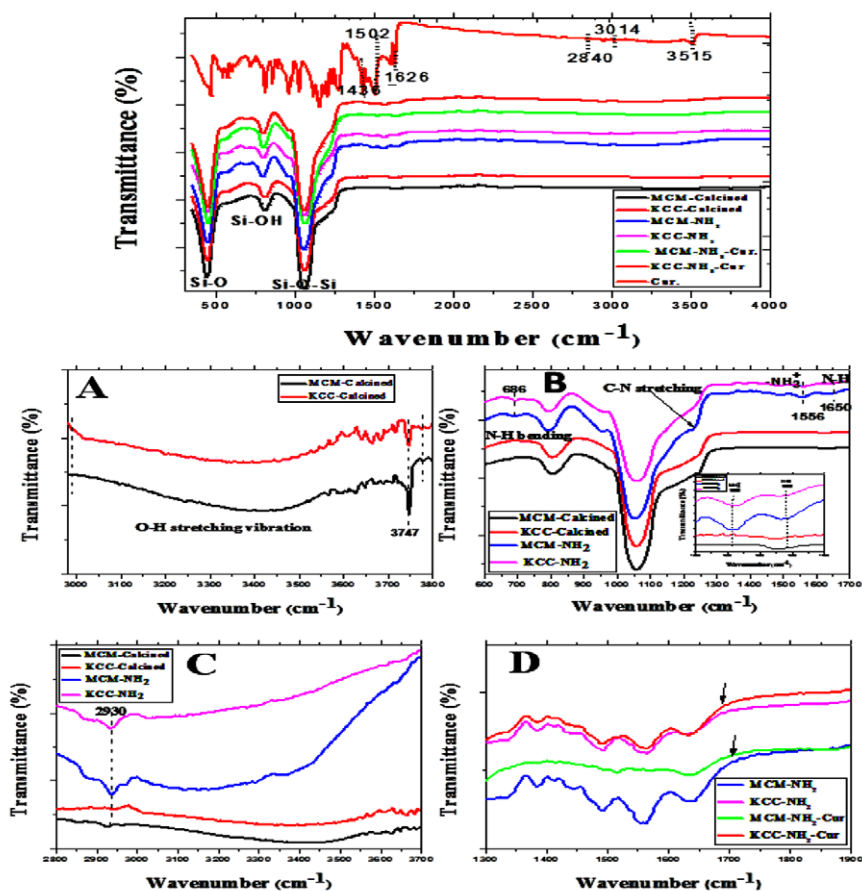


Figure 6: FTIR spectra of calcined, functionalized, Cur-loaded materials.

attributed to the symmetric and asymmetric configurations of C-O-C chains, peak at  $1436\text{ cm}^{-1}$  was attributed to CH<sub>2</sub> bending, while peak at  $1502\text{ cm}^{-1}$  was attributed to C=O and C=C vibration, peak at  $1626\text{ cm}^{-1}$  C=O stretching, peak at  $2840\text{ cm}^{-1}$  was assigned to C-H stretching of methyl group, peak at  $3014\text{ cm}^{-1}$  was due to C-H stretching of aromatic ring, and peak at  $3507\text{ cm}^{-1}$  was attributed to free -OH group vibration [36].

In MCM-NH<sub>2</sub>-Cur and KCC-NH<sub>2</sub>-Cur, a peak of (CH) of aromatic and skeletal CCH in pure Cur at  $790\text{ cm}^{-1}$  shifted towards  $800\text{ cm}^{-1}$  due to overlap with the band of Si-OH. In addition incorporation of Cur into the silica particles caused a marked decrease of amino groups' peaks (NH<sub>3</sub><sup>+</sup> and N-H), which may be due to the interaction between amino groups and Cur molecules (Figure 6D). FTIR spectra demonstrated that the adsorption/loading of Cur into functionalized silica materials had not physical manner, than confirmed that curcumin remained an amorphous form.

**Zeta potential measurements:** The surface charge of mesoporous silica particles can affect their performance as far as internalizing of cells, escaping endosomal entrapment [58] and also their load and sustained release [59,60]. As shown in Figure 7, all calcined, amine-functionalized and loaded silica nanoparticles showed positive zeta potential values in pH range from 2 to 2.5. It was noted that the KCC-NH<sub>2</sub>-Cur and MCM-NH<sub>2</sub>-Cur presented a higher positive zeta potential (+24 and +23.3, respectively) than calcined and functionalized samples. These results are consistent with previous data obtained by [61] when

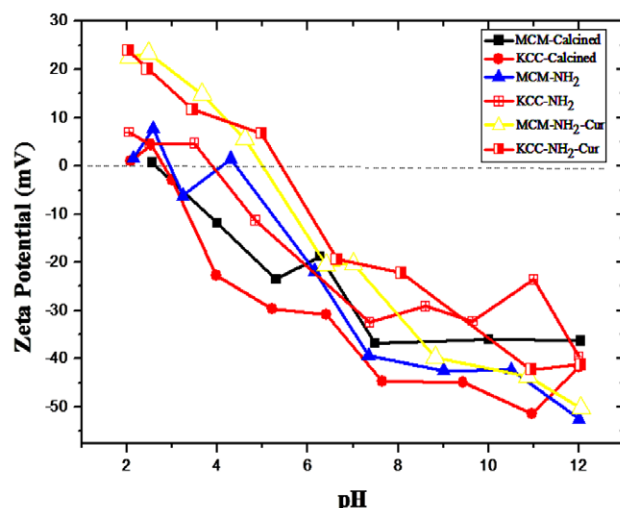


Figure 7: Zeta potential measurements of un-functionalized, functionalized and Cur-loaded mesoporous silica materials.

authors loaded anticancer drug to amine-modified MSMs. The drug-loaded silica material exhibited a higher positive zeta potential value as compared to amine-modified silica. This observation could further

provide evidence that the Cur-loaded silica materials would enhance their stability in aqueous media as compared to calcined and amine-functionalized silica particles. Although, the amine-modified particles showed slightly higher positive charges than calcined silica materials from pH 2 to 2.5. Similar trend was observed for modification with organic aminopropyl groups [62,63]. Under higher pH value up to 7.5, all samples exhibited a negative zeta potential with values of -37, -44, -40, -32, -23 and -20 in samples MCM-Calcined, KCC-Calcined, MCM-NH<sub>2</sub>, KCC-NH<sub>2</sub>, MCM-NH<sub>2</sub>-Cur and KCC-NH<sub>2</sub>-Cur, respectively. It was attributed to the fact that the silanol groups on the silica surface deprotonated, thereby all silica particles had a negative zeta potential values [60]. With further raising of pH up to 12, all samples exhibited negative charges values between -35 and -50.

### Qualitative analysis of the evolved gasses by STA-FTIR techniques

Simultaneous Thermal Analysis (STA) coupled with Fourier Transform Infrared spectroscopy (STA-FTIR), is a powerful tool for qualitative analysis of the gases evolved during the desorption or pyrolysis process [64-66]. Sensitivity of the FTIR is in the microgram range, while for ST it is 1 ug [67]. Therefore FTIR detect gasses even if the TG-curve does not show any mass changes of the sample. To our knowledge, this is the first time when STA-FTIR was used to characterize the gasses released during the heating of drug delivery system based on MSMs.

All types of samples were investigated using FTIR spectrometry coupled with STA apparatus. FTIR absorption three-dimensional spectra as a function of wave number and temperature are presented in Figure S3 of Supporting information. The FTIR absorbance spectra can be identified for selected temperature (reddish brown line) to show the gases released at specific condition, in accordance with TG results. For MCM-Calcined and KCC-Calcined samples mass decrease was observed at 220°C on TG curve. As it can be seen in Figures S3 A and B, this fall corresponds to release of: O-H stretch for water with a weaker intensity band (the range between 3600 and 3850 cm<sup>-1</sup>), CO<sub>2</sub> (the range between 2200 and 2400 cm<sup>-1</sup>), and H<sub>2</sub>O (the range between 1300 and 1700 cm<sup>-1</sup>).

A similar trend was found in amine-functionalized (MCM-NH<sub>2</sub> and KCC-NH<sub>2</sub>) samples as shown in Figures S3 C and 3D of Supporting information. At temperature around 450°C, the permanent gases evolved were: O-H for water, CO<sub>2</sub>, H<sub>2</sub>O, and CH<sub>4</sub> (the band around 400 cm<sup>-1</sup>). It was also noted that the functionalized-silica materials exhibited higher absorbance intensities than those of calcined samples. It could be due to attaching the organic aminopropyl molecules, consequently the CO<sub>2</sub> band presented the highest band intensity. Desorption of physically adsorbed water molecules was detected during the first mass loss below 100°C, while decomposition of aminopropyl groups in mesoporous materials was observed between 150-400°C [68,69].

In case of drug-loaded samples, the permanent release of O-H for water, CO<sub>2</sub>, and H<sub>2</sub>O was noted. However, both materials presented lower intensities, especially of CO<sub>2</sub>, as compared to the functionalized-materials. Moreover, KCC-NH<sub>2</sub>-Cur displayed an additional band, which may be due to CH<sub>4</sub> (the band around 400 cm<sup>-1</sup>). In case of drug-loaded samples we made an unexpected observation, namely that during heating, the samples showed gain losses instead of weight losses (the results are not shown). This phenomenon suggests that curcumin was not completely carbonized (decomposed) under the inert gas, helium. Moreover, we noted that after STA-FTIR analysis, the drug-loaded materials were still coloured in contrast to functionalized

samples. Subsequently we heated KCC-NH<sub>2</sub>-Cur and MCM-NH<sub>2</sub>-Cur materials again in air and noted that the samples became totally white. It proves, that the all organic molecules of drugs were finally released. In general the intensities of gases release increased with increasing the heating temperature. Water and CO<sub>2</sub> were released during the first mass loss step (evaporation of moisture) and final mass loss step (pyrolysis), especially in functionalized and drug loaded samples. During the pyrolysis gas release was more intensive of than during the first mass loss. The similar trend was detected for Cur sample as shown in Figure S3 (Supporting information).

### In vitro release and kinetic studies

The drug release studies were monitored for MCM-NH<sub>2</sub>-Cur and KCC-NH<sub>2</sub>-Cur and the release profiles are illustrated in Figure 8. The results showed that there was no initial burst release of curcumin in both materials. This could be attributed to the fact that the Cur molecules are loaded into mesopores, as was confirmed by XRD and DSC investigations were presented in Figures 4 and 5, respectively.

In general, as indicated in Figure 8, the Cur release from both silica materials was pH-dependent. At lower pH (2.5), the dissolution of Cur-loaded materials into release media was higher than for mildly acidic and neutral pH values of 5 and 7.5, respectively. Probably, under the low acidic condition (pH 2.5), the -NH<sub>2</sub> groups on the surface of silica nanoparticles become protonated, leading to more intense release as compared to the mildly acidic and neutral conditions. As shown in Figure 7, the Cur-loaded silica nanoparticles under low acidic condition from pH 2 up to 5 exhibited positive charge, while, under neutral pH condition (~7.5) negative. This may confirmed that the silica nanoparticles are protonated under low pH condition. In addition the release profiles of the examined materials were nearly linear.

Going further, as shown in Figures 8A and 8B, the cumulative release rates of Cur from silica materials during 100 h experiment were only about 14% in case of MCM-NH<sub>2</sub>-Cur, while about 19% in case of KCC-

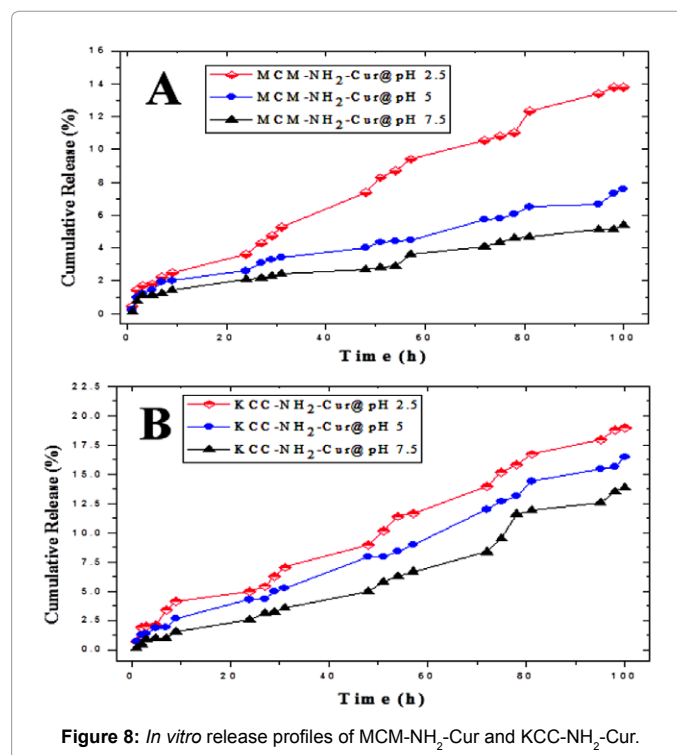


Figure 8: In vitro release profiles of MCM-NH<sub>2</sub>-Cur and KCC-NH<sub>2</sub>-Cur.

NH<sub>2</sub>-Cur. Furthermore, Cur release has not reached the equilibrium state, and may be continued for long time to reach the equilibrium. Such a difference between the two materials may be due to the difference in the pore size distribution. MCM-41 material exhibits a sharp peak of small pore size (nearly 2 nm) as shown in Figure 2. On the other hand the KCC-1 nanoparticles possess a fibrous structure with dendrimeric mesopores, with wide range of pore size up to 5 nm. Therefore the release profiles of both samples were influenced by the pore size of the MSNs and the curcumin release from KCC-1 is more intensive compared to MCM-41. This finding is in accordance with earlier study made for celecoxib as the drug loaded with 3D face-centered cubic mesoporous silica [46]. It was reported that the structural factors such as internal pore structure, surface area of mesoporous nanoparticles determine the controlled release of drug molecules via accessibility and mobility inside pore matrices [70,71]. It has been previously pointed that drug diffusion from MSNs is related to the pore diameter, i.e., the smaller mesopores size the smaller kinetic release constant [15]. Also pore geometry can affect diffusion coefficients of MSNs, which would be larger in 3D than 2D structures [70]. It was reported that the silica nanoparticles functionalized with aminopropyl groups are suitable for regulated and controlled release of Cur. It could be attributed to relatively slight hydrophobicity owing to the aminopropyl chain of APTES, leading to slower influx of liquid media into the pores, finally delaying the dissolution of Cur [36]. In addition, APTES would impart some steric hindrance inhibiting the release of Cur from mesopores of nanoparticles [72]. Also, by employing amino-functionalized silica nanoparticles, the release of emodin drug is also controlled [73]. It can be concluded that morphology of the amine-functionalized mesoporous silica materials play a principle role in the modulating of curcumin release. Thus, this kind of release system shows long-term release; therefore it could be beneficial in biomedical applications. For instance in cancer therapy, because of acidic tumor environment [74].

To analyze the *in vitro* release profiles data, several kinetic models can be used. In some studies, the Higuchi model was used [75-78], in other cases, the first-order kinetic exponential decay model was employed [51,71,75], the Korsmeyer-Peppas model was used [79-81], or the Zero-order model with other models were utilized [82,83]. In our study, kinetic models for curcumin kinetic release studies were chosen: Zero-order, first order and Higashi kinetic models, while the Kmeyer-Peppas model was used to describe the release mechanism of curcumin from nanoparticles. The obtained cumulative % of Cur release data were fitted in all models, the estimation was performed with the DDSolver software [84]. The parameters of K0 (zero-order release constant), K1 (first-order release constant), KH (Higashi model release constant) and R<sup>2</sup> (coefficient of determination) obtained after fitting the Cur release data with all three models are listed in Table 2. It can be seen that, the kinetic release of Cur from two materials depends on the MSNs type and the pH of release medium. The R<sup>2</sup> values obtained for MCM-NH<sub>2</sub>-Cur was equal to 0.90 or higher than up to 0.941, which

indicated that the Cur release from this type good fit to Higushi model. Moreover, the KH values decreased with increasing the pH level: they were 1.206, 0.651 and 0.475 for pH 2.5, 5 and 7.5, respectively. The decrease of KH values with increase of pH demonstrate that for higher pH level Cur release rate is decreasing. In the case of KCC-NH<sub>2</sub>-Cur this model did not allowed for a good fit, since the R<sup>2</sup> values not reach 0.90. On the other hand, when the Zero-order model was applied, the R<sup>2</sup> values obtained for KCC-NH<sub>2</sub>-Cur were equal to or higher than 0.964, indicating good fit. Again, the K0 values decreased by 0.194, 0.162 and 0.129 with increasing the pH level from 2.5, 5 and 7.5, respectively. This observation also indicates that increase of Ph leads to slower Cur release in the case of this material as well. It was also noted that, the release kinetics for MCC-NH<sub>2</sub>-Cur fits perfectly to this model only under acidic pH condition (2.5), since the R<sup>2</sup> value was 0.97. In case of fitting the release data of Cur release to the first-order model, it is observed that the KCC-NH<sub>2</sub>-Cur showed good fit to this model, but K1 values were very small. While, the MCM-NH<sub>2</sub>-Cur showed only good fit to this model only at pH condition 2.5 (R<sup>2</sup>=0.974). However, the small values obtained with first-order model suggesting that some of Cur molecules exhibited a burst release effect at the initial state of releasing process. These results confirm that the curcumin release kinetics is dependent on the type of silica nanoparticles and the pH of release medium. Since the morphology structure of nanocarriers determine the interface between drug-loaded systems and the release medium, leading to influence the drug release kinetics [85-88]. It can be conclude that, mainly the delivery system of curcumin from both materials can be fitted to Higuchi model for MCM-NH<sub>2</sub>-Cur, and fitted to zero-order model for KCC-NH<sub>2</sub>-Cur.

To understand the drug release mechanism of our delivery system, the Korsmeyer-Peppas model [89] was employed (see equation 1).

$$Mt/M_{\infty}=kt^n \quad (1)$$

Where Mt and M<sub>∞</sub> denote the cumulative mass of drug released at time t and at infinite time, respectively; K is a kinetic constant characteristic of the drug-carrier system; and n is an exponent (release index), which is indicative of the mechanism of the drug release. The release index n gives the information about the release mechanism of drug; n ≤ 0.45, represents a Fickian Diffusion [90]. If n > 0.45 and < 0.89, a non-Fickian or anomalous diffusion is present; n = 0.89, provides a case II transport, while n > 0.89, indicates a zero-order mechanism [91].

The release data were fitted to this model from both materials under different pH conditions and presented in in Table 3. The results indicated that all materials good fit to Korsmeyer-Peppas model, since all R<sup>2</sup> values were in the range from 0.956 to 0.981. In case of MCM-NH<sub>2</sub>-Cur system, the n values were 0.841, 0.634 and 0.651 under pH condition of 2.5, 5 1 and 7.5 respectively. These results indicate that the curcumin release mechanism from this system follows non-Fickian or anomalous diffusion. In the case of KCC-NH<sub>2</sub>-Cur system, the n values

Material	pH	Zero Order		First Order		Higuchi	
		R <sup>2</sup>	K0 (%·h <sup>-1</sup> )	R <sup>2</sup>	K1(%·h <sup>-1</sup> )	R <sup>2</sup>	KH (%·h <sup>-1</sup> )
MCM-NH <sub>2</sub> -Cur	2.5	0.9698	0.148	0.9743	0.002	0.9004	1.206
KCC-NH <sub>2</sub> -Cur	2.5	0.9706	0.194	0.971	0.002	0.8707	1.58
MCM-NH <sub>2</sub> -Cur	5	0.8776	0.078	0.8845	0.001	0.9415	0.651
KCC-NH <sub>2</sub> -Cur	5	0.9775	0.162	0.9755	0.002	0.8515	1.312
MCM-NH <sub>2</sub> -Cur	7.5	0.8847	0.057	0.8893	0.001	0.9337	0.475
KCC-NH <sub>2</sub> -Cur	7.5	0.9645	0.129	0.9588	0.001	0.7914	1.029

R<sup>2</sup>: correlation coefficient, K0: zero-order rate constant, K1: first-order rate constant, KH: Higuchi rate constant

**Table 2:** Kinetic parameters of curcumin release from silica materials as drug carrier systems under different pH conditions based on several mathematical models.

Material	pH	Korsmeyer-Peppas model			Mechanism
		K(h <sup>-n</sup> )	R <sup>2</sup>	n	
MCM-NH <sub>2</sub> -Cur	2.5	0.292	0.9810	0.841	non-Fickian or anomalous diffusion
KCC-NH <sub>2</sub> -Cur	2.5	0.272	0.9729	0.921	zero-order mechanism
MCM-NH <sub>2</sub> -Cur	5	0.375	0.9607	0.634	non-Fickian or anomalous diffusion
KCC-NH <sub>2</sub> -Cur	5	0.164	0.9775	0.998	zero-order mechanism
MCM-NH <sub>2</sub> -Cur	7.5	0.255	0.9565	0.651	non-Fickian or anomalous diffusion
KCC-NH <sub>2</sub> -Cur	7.5	0.053	0.9751	1.205	zero-order mechanism

K: rate constant, R: correlation coefficient, n: release exponent

**Table 3:** The Korsmeyer–Peppas model fits of curcumin release from two types of MSNs under different pH conditions.

were 0.921, 0.998 and 1.205 with pH values 2.5, 5 and 7.5, respectively. This observation, demonstrates that the Cur release mechanism from this system follows zero-order mechanism. Hence, it was demonstrated that the release mechanism of curcumin depends on type of mesoporous silica nanoparticles. This could be due to the described above fact that both of silica types exhibit different morphology structures. The differences in physicochemical properties such the surface area and porosity determine the drug release mechanism via influence the accessibility and mobility of drug molecules inside the pores of silica material and then their release behaviour [71,92].

## Conclusion

The pH-controlled release of anticancer model natural pro-drug Curcumin was achieved by using of Two-Dimensional (MCM-41) and Three-Dimensional (KCC-1) mesoporous silica with aminopropyl functional groups. The drug-loaded materials were characterized using several techniques and it was confirmed that the curcumin was loaded into internal pores in amorphous state, which could lead to enhancing its solubility. The results showed that the loading capacity of Cur was similar in KCC-NH<sub>2</sub>-Cur and MCM-NH<sub>2</sub>-Cur. During *in vitro* release experiments, and in low acidity conditions of pH 2,5, KCC-NH<sub>2</sub>-Cur exhibited higher release rate compared to MCM-NH<sub>2</sub>-Cur. The lower release kinetics of MCM-NH<sub>2</sub>-Cur could be attributed to smaller and narrow pore size distribution in the range of 2 nm. Kinetic release studies using several mathematical models, confirmed that the kinetic of release of curcumin depends on the type of silica nanoparticles and the level pH in the release medium. The Higuchi model provides a good fit for MCM-NH<sub>2</sub>-Cur, where release is controlled by a non-Fickian or anomalous diffusion mechanism. The zero-order model provides a good fit for KCC-NH<sub>2</sub>-Cur, where the zero-order release mechanism takes place. Thus, the structural properties of silica nanoparticles play very important role in enhancement of the release of poorly-water soluble curcumin as anticancer drug. This system also demonstrated a long-term release, which is important for its anticancer activity, and can be utilized in targeted drug delivery system in cancer therapy. Especially KCC-1 mesoporous silica seems to open new opportunities for controlled delivery system in the near future.

## Acknowledgements

This work was supported by the National Research Centre (NRC), Egypt. We thank the Laboratory of Nanostructures for Photonic and Nanomedicine, Polish Academy of Sciences, Poland, as well as, the Academy of Scientific Research and Technology, Egypt.

## References

- Zhang Y, Chan HF, Leong KW (2013) Advanced materials and processing for drug delivery: the past and the future. *Adv Drug Deliv Rev* 65: 104-120.
- Vallet-Regi M, Rámila A, del Real RP, Pérez-Pariente J (2001) A New Property of MCM-41: Drug Delivery System. *Chemistry of Materials* 13: 308-311.

- Ambrogio MW, Thomas CR, Zhao YL, Zink JI, Stoddart JF (2011) Mechanized silica nanoparticles: a new frontier in theranostic nanomedicine. *Acc Chem Res* 44: 903-913.
- Fontecave T, Sanchez C, Azaïs T, Boissière C (2012) Chemical Modification As a Versatile Tool for Tuning Stability of Silica Based Mesoporous Carriers in Biologically Relevant Conditions. *Chemistry of Materials* 24: 4326-4336.
- Manzano M, Aina V, Areán CO, Balas F, Cauda V, et al. (2008) Studies on MCM-41 mesoporous silica for drug delivery: Effect of particle morphology and amine functionalization. *Chemical Engineering Journal* 137: 30-37.
- Rosenholm JM, Sahlgrén C, Linden M (2010) Towards multifunctional, targeted drug delivery systems using mesoporous silica nanoparticles - opportunities & challenges. *Nanoscale* 2: 1870-1883.
- Santamaría E, Maestro A, Porras M, Gutiérrez JM, González C (2014) Controlled release of ibuprofen by meso-macroporous silica. *Journal of Solid State Chemistry* 210: 242-250.
- Wang X, Liu Y, Wang S, Shi D, Zhou X, et al. (2015) CD44-engineered mesoporous silica nanoparticles for overcoming multidrug resistance in breast cancer. *Applied Surface Science* 332: 308-317.
- Yan H, Teh C, Sreejith S, Zhu L, Kwok A, et al. (2012) Functional Mesoporous Silica Nanoparticles for Photothermal-Controlled Drug Delivery *In Vivo*. *Angewandte Chemie International Edition* 51: 8373-8377.
- Aghaei H, Nourbakhsh AA, Karbasi S, JavadKalbasi R, Rafienia M, et al. (2014) Investigation on bioactivity and cytotoxicity of mesoporous nano-composite MCM-48/hydroxyapatite for ibuprofen drug delivery. *Ceramics International* 40: 7355-7362.
- Areán CO, Vesga MJ, Parra JB, Delgado MR (2013) Effect of amine and carboxyl functionalization of sub-micrometric MCM-41 spheres on controlled release of cisplatin. *Ceramics International* 39: 7407-7414.
- Min Z, Yufang Z, Lingxia Z, Jianlin S (2013) Preparation of chitosan/mesoporous silica nanoparticle composite hydrogels for sustained co-delivery of biomacromolecules and small chemical drugs. *Science and Technology of Advanced Materials* 14: 045005.
- Ashley CE, Carnes EC, Phillips GK, Padilla D, Durfee PN, et al. (2011) The targeted delivery of multicomponent cargos to cancer cells by nanoporous particle-supported lipid bilayers. *Nat Mater* 10: 389-397.
- Slowing II, Vivero-Escoto JL, Trewyn BG, Lin VSY (2010) Mesoporous silica nanoparticles: structural design and applications. *Journal of Materials Chemistry* 20: 7924-7937.
- Vallet-Regi M, Balas F, Arcos D (2007) Mesoporous materials for drug delivery. *Angew Chem Int Ed Engl* 46: 7548-7558.
- Polshettiwar V, Cha D, Zhang X, Basset JM (2010) High-Surface-Area Silica Nanospheres (KCC-1) with a Fibrous Morphology. *Angewandte Chemie International Edition* 49: 9652-9656.
- Salem M, Rohani S, Gillies ER (2014) Curcumin, a promising anti-cancer therapeutic: a review of its chemical properties, bioactivity and approaches to cancer cell delivery. *RSC Advances* 4: 10815-10829.
- Ak T, Gülçin I (2008) Antioxidant and radical scavenging properties of curcumin. *Chem Biol Interact* 174: 27-37.
- Sandur SK, Pandey MK, Sung B, Ahn KS, Murakami A, et al. (2007) Curcumin, demethoxycurcumin, bisdemethoxycurcumin, tetrahydrocurcumin and turmerones differentially regulate anti-inflammatory and anti-proliferative responses through a ROS-independent mechanism. *Carcinogenesis* 28: 1765-1773.

20. Mun SH, Joung DK, Kim YS, Kang OH, Kim SB, et al. (2013) Synergistic antibacterial effect of curcumin against methicillin-resistant *Staphylococcus aureus*. *Phytomedicine* 20: 714-718.
21. Ghoneum M, Gollapudi S (2011) Synergistic apoptotic effect of arabinoxylan rice bran (MGN-3/Biobran) and curcumin (turmeric) on human multiple myeloma cell line U266 *in vitro*. *Neoplasma* 58: 118-123.
22. Wilken R, Veena MS, Wang MB, Srivatsan ES (2011) Curcumin: A review of anti-cancer properties and therapeutic activity in head and neck squamous cell carcinoma. *Mol Cancer* 10: 12.
23. Aggarwal BB (2008) Prostate cancer and curcumin: add spice to your life. *Cancer Biol Ther* 7: 1436-1440.
24. Anand P, Kunnumakkara AB, Newman RA, Aggarwal BB (2007) Bioavailability of curcumin: problems and promises. *Mol Pharm* 4: 807-818.
25. Gupta SC, Kismali G, Aggarwal BB (2013) Curcumin, a component of turmeric: from farm to pharmacy. *Biofactors* 39: 2-13.
26. Shehzad A, Lee J, Lee YS (2013) Curcumin in various cancers. *Biofactors* 39: 56-68.
27. Siviero A, Gallo E, Maggini V, Gori L, Mugelli A, et al. (2015) Curcumin, a golden spice with a low bioavailability. *Journal of Herbal Medicine* 5: 57-70.
28. Anand P, Thomas SG, Kunnumakkara AB, Sundaram C, Harikumar KB, et al. (2008) Biological activities of curcumin and its analogues (Congeners) made by man and Mother Nature. *Biochem Pharmacol* 76: 1590-1611.
29. Bharali DJ, Siddiqui IA, Adhami VM, Chamcheu JC, Aldahmash AM, et al. (2011) Nanoparticle delivery of natural products in the prevention and treatment of cancers: current status and future prospects. *Cancers (Basel)* 3: 4024-4045.
30. Oussoren C, Storm G (2001) Liposomes to target the lymphatics by subcutaneous administration. *Adv Drug Deliv Rev* 50: 143-156.
31. Uhrich KE, Cannizzaro SM, Langer RS, Shakesheff KM (1999) Polymeric systems for controlled drug release. *Chem Rev* 99: 3181-3198.
32. Wang YJ, Pan MH, Cheng AL, Lin LI, Ho YS, et al. (1997) Stability of curcumin in buffer solutions and characterization of its degradation products. *J Pharm Biomed Anal* 15: 1867-1876.
33. Pawar YB, Shete G, Popat D, Bansal AK (2012) Phase behavior and oral bioavailability of amorphous Curcumin. *Eur J Pharm Sci* 47: 56-64.
34. Kaushal AM, Gupta P, Bansal AK (2004) Amorphous drug delivery systems: molecular aspects, design, and performance. *Crit Rev Ther Drug Carrier Syst* 21: 133-193.
35. Jambhrunkar S, Karmakar S, Popat A, Yu M, Yu C (2014) Mesoporous silica nanoparticles enhance the cytotoxicity of curcumin. *RSC Advances* 4: 709-712.
36. Jambhrunkar S, Qu Z, Popat A, Yang J, Noonan O, et al. (2014) Effect of surface functionality of silica nanoparticles on cellular uptake and cytotoxicity. *Mol Pharm* 11: 3642-3655.
37. Ma'mani L, Nikzad S, Kheiri-manjili H, al-Musawi S, Saeedi M, et al. (2014) Curcumin-loaded guanidine functionalized PEGylated I3ad mesoporous silica nanoparticles KIT-6: Practical strategy for the breast cancer therapy. *European Journal of Medicinal Chemistry* 83: 646-654.
38. Jin D, Lee JH, Seo ML, Jaworski J, Jung JH (2012) Controlled drug delivery from mesoporous silica using a pH-response release system. *New Journal of Chemistry* 36: 1616-1620.
39. Jin D, Park KW, Lee JH, Song K, Kim JG, et al. (2011) The selective immobilization of curcumin onto the internal surface of mesoporous hollow silica particles by covalent bonding and its controlled release. *Journal of Materials Chemistry* 21: 3641-3645.
40. Lu J, Li Z, Zink JL, Tamanoi F (2012) In vivo tumor suppression efficacy of mesoporous silica nanoparticles-based drug-delivery system: enhanced efficacy by folate modification. *Nanomedicine: Nanotechnology, Biology and Medicine* 8: 212-220.
41. Moon DS, Lee JK (2012) Tunable synthesis of hierarchical mesoporous silica nanoparticles with radial wrinkle structure. *Langmuir* 28: 12341-12347.
42. Huang X, Tao Z, Praskavich JC Jr, Goswami A, Al-Sharab JF, et al. (2014) Dendritic silica nanomaterials (KCC-1) with fibrous pore structure possess high DNA adsorption capacity and effectively deliver genes *in vitro*. *Langmuir* 30: 10886-10898.
43. Limnell T, Santos HA, Mäkilä E, Heikkilä T, Salonen J, et al. (2011) Drug delivery formulations of ordered and nonordered mesoporous silica: comparison of three drug loading methods. *J Pharm Sci* 100: 3294-3306.
44. Popova M, Szegedi A, Yoncheva K, Konstantinov S, Petrova GP, et al. (2014) New method for preparation of delivery systems of poorly soluble drugs on the basis of functionalized mesoporous MCM-41 nanoparticles. *Microporous and Mesoporous Materials* 198: 247-255.
45. Wu C, Sun X, Zhao Z, Zhao Y, Hao Y, et al. (2014) Synthesis of novel core-shell structured dual-mesoporous silica nanospheres and their application for enhancing the dissolution rate of poorly water-soluble drugs. *Materials Science and Engineering: C* 44: 262-267.
46. Zhu W, Wan L, Zhang C, Gao Y, Zheng X, et al. (2014) Exploitation of 3D face-centered cubic mesoporous silica as a carrier for a poorly water soluble drug: influence of pore size on release rate. *Mater Sci Eng C Mater Biol Appl* 34: 78-85.
47. Mani G, Pushparaj H, Peng MM, Muthiahpillai P, Udhumasha U, et al. (2014) Synthesis and characterization of pharmaceutical surfactant templated mesoporous silica: Its application to controlled delivery of duloxetine. *Materials Research Bulletin* 51: 228-235.
48. Li-Hong W, Xin C, Hui X, Li-Li Z, Jing H, et al. (2013) A novel strategy to design sustained-release poorly water-soluble drug mesoporous silica microparticles based on supercritical fluid technique. *Int J Pharm* 454: 135-142.
49. Charnay C, Bégu S, Tourné-Péteilh C, Nicole L, Lerner DA, et al. (2004) Inclusion of ibuprofen in mesoporous templated silica: drug loading and release property. *Eur J Pharm Biopharm* 57: 533-540.
50. Chong ASM, Zhao XS (2003) Functionalization of SBA-15 with APTES and Characterization of Functionalized Materials. *The Journal of Physical Chemistry B* 107: 12650-12657.
51. Datt A, El-Maazawi I, Larsen SC (2012) Aspirin Loading and Release from MCM-41 Functionalized with Aminopropyl Groups via Co-condensation or Postsynthesis Modification Methods. *The Journal of Physical Chemistry C* 116: 18358-18366.
52. Gai S, Yang P, Ma P, Wang L, Li C, et al. (2012) Uniform and size-tunable mesoporous silica with fibrous morphology for drug delivery. *Dalton Trans* 41: 4511-4516.
53. Gayam SR, Wu SP (2014) Redox responsive Pd(ii) templated rotaxane nanovalve capped mesoporous silica nanoparticles: a folic acid mediated biocompatible cancer-targeted drug delivery system. *Journal of Materials Chemistry* 2: 7009-7016.
54. White LD, Tripp CP (2000) An Infrared Study of the Amine-Catalyzed Reaction of Methoxymethylsilanes with Silica. *J Colloid Interface Sci* 227: 237-243.
55. Szegedi A, Popova M, Goshev I, Mihály J (2011) Effect of amine functionalization of spherical MCM-41 and SBA-15 on controlled drug release. *Journal of Solid State Chemistry* 184: 1201-1207.
56. Mangolim CS, Moriwaki C, Nogueira AC, Sato F, Baesso ML, et al. (2014) Curcumin- $\beta$ -cyclodextrin inclusion complex: stability, solubility, characterisation by FT-IR, FT-Raman, X-ray diffraction and photoacoustic spectroscopy, and food application. *Food Chem* 153: 361-370.
57. Kolev TM, Velcheva EA, Stamboliyska BA, Spitteller M (2005) DFT and experimental studies of the structure and vibrational spectra of curcumin. *International Journal of Quantum Chemistry* 102: 1069-1079.
58. Chung TH, Wu SH, Yao M, Lu CW, Lin YS, et al. (2007) The effect of surface charge on the uptake and biological function of mesoporous silica nanoparticles in 3T3-L1 cells and human mesenchymal stem cells. *Biomaterials* 28: 2959-2966.
59. DeMuth P, Hurley M, Wu C, Galanie S, Zachariah MR, et al. (2011) Mesoporous silica as drug delivery vehicles: Synthesis, characterization, and pH-sensitive release profiles. *Microporous and Mesoporous Materials* 141: 128-134.
60. Lee CH, Lo LW, Mou CY, Yang CS (2008) Synthesis and Characterization of Positive-Charge Functionalized Mesoporous Silica Nanoparticles for Oral Drug Delivery of an Anti-Inflammatory Drug. *Advanced Functional Materials* 18: 3283-3292.
61. Wani A, Muthuswamy E, Savithra GL, Mao G, Brock S, et al. (2012) Surface Functionalization of Mesoporous Silica Nanoparticles Controls Loading and Release Behavior of Mitoxantrone. *Pharmaceutical Research* 29: 2407-2418.

62. Popat A, Jambhrunkar S, Zhang J, Yang J, Zhang H, et al. (2014) Programmable drug release using bioresponsive mesoporous silica nanoparticles for site-specific oral drug delivery. *Chem Commun (Camb)* 50: 5547-5550.
63. Yoncheva K, Popova M, Szegedi A, Mihaly J, Tzankov B, et al. (2014) Functionalized mesoporous silica nanoparticles for oral delivery of budesonide. *Journal of Solid State Chemistry* 211: 154-161.
64. Marcilla A, Gómez A, Menargues S (2005) TGA/FTIR study of the evolution of the gases evolved in the catalytic pyrolysis of ethylene-vinyl acetate copolymers. Comparison among different catalysts. *Polymer Degradation and Stability* 89: 454-460.
65. Rogaume T, Valencia LB, Guillaume E, Richard F, Luche J, et al. (2011) Development of the Thermal Decomposition Mechanism of Polyether Polyurethane Foam Using Both Condensed and Gas-Phase Release Data. *Combustion Science and Technology* 183: 627-644.
66. Schindler A, Neumann G, Rager A, Füglein E, Blumm J, et al. (2013) A novel direct coupling of simultaneous thermal analysis (STA) and Fourier transform-infrared (FT-IR) spectroscopy. *Journal of Thermal Analysis and Calorimetry* 113: 1091-1102.
67. Akinade KA, Campbell RM, Compton DC (1994) The use of a simultaneous TGA/DSC/FT-IR system as a problem-solving tool. *Journal of Materials Science* 29: 3802-3812.
68. Parida KM, Rath D (2009) Amine functionalized MCM-41: An active and reusable catalyst for Knoevenagel condensation reaction. *Journal of Molecular Catalysis A: Chemical* 310: 93-100.
69. Vunain E, Opembe N, Jalama K, Mishra A, Meijboom R (2014) Thermal stability of amine-functionalized MCM-41 in different atmospheres. *Journal of Thermal Analysis and Calorimetry* 115: 1487-1496.
70. Brohede U, Alturi R, Garcia-Bennett AE, Strømme M (2008) Sustained release from mesoporous nanoparticles: evaluation of structural properties associated with release rate. *Curr Drug Deliv* 5: 177-185.
71. Nieto A, Colilla M, Balas F, Vallet-Regí M (2010) Surface electrochemistry of mesoporous silicas as a key factor in the design of tailored delivery devices. *Langmuir* 26: 5038-5049.
72. Jal PK, Patel S, Mishra BK (2004) Chemical modification of silica surface by immobilization of functional groups for extractive concentration of metal ions. *Talanta* 62: 1005-1028.
73. Xu Y, Wang C, Zhou G, Wu Y, Chen J (2012) Improving the controlled release of water-insoluble emodin from amino-functionalized mesoporous silica. *Applied Surface Science* 258: 6366-6372.
74. Colilla M, Gonzalez B, Vallet-Regi M (2013) Mesoporous silica nanoparticles for the design of smart delivery nanodevices. *Biomaterials Science* 1: 114-134.
75. Costa P, Sousa Lobo JM (2001) Modeling and comparison of dissolution profiles. *Eur J Pharm Sci* 13: 123-133.
76. Horcajada P, Márquez-Alvarez C, Rámila A, Pérez-Pariente J, Vallet-Regí M (2006) Controlled release of Ibuprofen from dealuminated faujasites. *Solid State Sciences* 8: 1459-1465.
77. Aznar E, Sancenón F, Marcos MD, Martínez-Máñez R, Stroeve P, et al. (2012) Delivery modulation in silica mesoporous supports via alkyl chain pore outlet decoration. *Langmuir* 28: 2986-2996.
78. Nadrah P, Maver U, Jemec A, Tišler T, Bele M, et al. (2013) Hindered Disulfide Bonds to Regulate Release Rate of Model Drug from Mesoporous Silica. *ACS Applied Materials and Interfaces* 5: 3908-3915.
79. Gao L, Sun J, Zhang L, Li Y, Ren B (2011) Thermal decomposition behavior of amino groups modified bimodal mesoporous silicas as aspirin carrier. *J Nanosci Nanotechnol* 11: 10324-10332.
80. Popovici RF, Seftel EM, Mihai GD, Popovici E, Voicu VA (2011) Controlled drug delivery system based on ordered mesoporous silica matrices of captopril as angiotensin-converting enzyme inhibitor drug. *J Pharm Sci* 100: 704-714.
81. Zhu Yf, Shi JL, Li YS, Chen HR, Shen WH, et al. (2005) Storage and release of ibuprofen drug molecules in hollow mesoporous silica spheres with modified pore surface. *Microporous and Mesoporous Materials* 85: 75-81.
82. Carriazo D, del Arco M, Fernández A, Martín C, Rives V (2010) Inclusion and release of fenbufen in mesoporous silica. *J Pharm Sci* 99: 3372-3380.
83. Liu F, Wang J, Cao Q, Deng H, Shao G, et al. (2015) One-step synthesis of magnetic hollow mesoporous silica (MHMS) nanospheres for drug delivery nanosystems via electrostatic self-assembly templated approach. *Chem Commun (Camb)* 51: 2357-2360.
84. Zhang Y, Huo M, Zhou J, Zou A, Li W, et al. (2010) DDSolver: an add-in program for modeling and comparison of drug dissolution profiles. *AAPS J* 12: 263-271.
85. Slowing II, Vivero-Escoto JL, Wu CW, Lin VS (2008) Mesoporous silica nanoparticles as controlled release drug delivery and gene transfection carriers. *Adv Drug Deliv Rev* 60: 1278-1288.
86. Lin CX, Qiao SZ, Yu CZ, Ismadij S, Lu GQ (2009) Periodic mesoporous silica and organosilica with controlled morphologies as carriers for drug release. *Microporous and Mesoporous Materials* 117: 213-219.
87. Qu F, Zhu G, Huang S, Li S, Sun J, et al. (2006) Controlled release of Captopril by regulating the pore size and morphology of ordered mesoporous silica. *Microporous and Mesoporous Materials* 92: 1-9.
88. Guo Z, Liu XM, Ma L, Li J, Zhang H, et al. (2013) Effects of particle morphology, pore size and surface coating of mesoporous silica on Naproxen dissolution rate enhancement. *Colloids Surf B Biointerfaces* 101: 228-235.
89. Korsmeyer RW, Gurny R, Doelker E, Buri P, Peppas NA (1983) Mechanisms of solute release from porous hydrophilic polymers. *International Journal of Pharmaceutics* 15: 25-35.
90. Ritger PL, Peppas NA (1987) A simple equation for description of solute release I. Fickian and non-fickian release from non-swellable devices in the form of slabs, spheres, cylinders or discs. *Journal of Controlled Release* 5: 23-36.
91. Peppas NA (1985) Analysis of Fickian and non-Fickian drug release from polymers. *Pharm Acta Helv* 60: 110-111.
92. Ukmar T, Maver U, Planinšek O, Kaučič V, Gaberšček M, Godec A (2011) Understanding controlled drug release from mesoporous silicates: theory and experiment. *J Control Release* 155: 409-417.